Powder flow and deposition profile in directed energy deposition with discrete coaxial injection

Aji Nugroho[1*], *Shu-San* Hsiau[2], *Li-Tsung* Sheng[3], *Bing-Zhi* Wang[2], *Firman* Yasa Utama[1], and *Dyah* Riandadari[1]

[1]Applied Mechanical Engineering, Faculty of Vocational Studies, Universitas Negeri Surabaya, Indonesia
[2]Department of Mechanical Engineering, National Central University, Jhongli, Taiwan
[3]Department of Mechanical and Electro-Mechanical Engineering, National Ilan University, Yilan, Taiwan

Abstract. This study explores the effects of powder injection angle and substrate inclination on powder flow characteristics and deposition profiles in Directed Energy Deposition (DED) using a discrete coaxial nozzle. A multiphase simulation based on the Euler-Lagrange method and Discrete Phase Modeling (DPM) was performed to evaluate particle trajectories, velocity, focal convergence, and deposition geometry across five injection angles (110°–135°) and four substrate inclinations (0°–60°). The results reveal that lower injection angles produce a more stable and focused powder stream, improving deposition quality and efficiency. In contrast, angles above 130° reduce focal precision due to increased divergence and particle collisions. Substrate inclinations greater than 40° shift the peak deposition point and reduce cladding uniformity, indicating sensitivity to geometric orientation. These findings contribute to precision control strategies for DED processes, particularly in complex remanufacturing tasks. As metal additive manufacturing expands in the aerospace industry, integrating artificial intelligence for real-time monitoring and adaptive control can enhance process reliability, reduce material waste, and enable autonomous repairs. The study demonstrates that careful tuning of injection parameters is essential to meet the high-performance demands of next-generation remanufacturing systems.

1 Introduction

Metal additive manufacturing (AM) continues to transform industrial production by enabling the creation and repair of complex components with minimal material waste and enhanced geometric flexibility [1]. Among the various AM techniques, Directed Energy Deposition (DED) stands out for its capability to add material directly onto existing parts, making it particularly relevant in the aerospace sector, where remanufacturing worn or damaged high-value components is both cost-effective and critical for operational safety [2], [3]. DED achieves this by simultaneously melting and depositing metal feedstock—often in powder form—using a high-energy heat source, offering localized control over the build process [4].

An essential challenge in DED lies in controlling powder flow and ensuring precise material placement[5], [6], [7]. Powder stream behavior, convergence, and interaction with the substrate directly affect deposition efficiency, track morphology, and the mechanical performance of the final build. These aspects are particularly sensitive to the injection angle of the powder and the orientation of the substrate, both of which can vary significantly in real-world remanufacturing applications [8], [9]. For instance, aircraft components requiring surface restoration often have curved or tilted geometries, which complicate consistent material delivery.

While many studies have examined coaxial powder flow in idealized horizontal configurations, limited research has focused on the effect of varying injection angles in conjunction with inclined substrates, especially in systems using discrete coaxial nozzles. These nozzles, which deliver powder from separate ports arranged around the central axis, are advantageous for their directional control and compact design, making them suitable for repairing complex geometries [10]. However, their behavior under angular misalignment remains poorly understood, representing a clear gap in the current knowledge base.

DED relies on precise control of powder flow within a turbulent multiphase field, where drag, gravity, and interparticle collisions govern the stability and accuracy of material deposition. In discrete coaxial injection systems, small deviations in injection geometry can disrupt focal convergence and reduce capture efficiency, resulting in irregular cladding morphology and surface nonuniformity. These effects are especially critical in aerospace remanufacturing, where deposition precision directly influences structural integrity and repair performance [11], [12].

Although several studies have investigated coaxial powder flow under ideal horizontal configurations, the combined influence of injection angle and substrate inclination has not been comprehensively analyzed.

* Corresponding author: nugrohoaji@unesa.ac.id

Understanding this interaction is essential for advancing adaptive DED systems capable of compensating for complex geometries and ensuring uniform material delivery [13], [14].

The research contribution of this study is to establish a quantitative and physics-based understanding of how variations in powder-injection angle and substrate inclination jointly affect powder-flow dynamics and deposition morphology. Through validated multiphase numerical simulations, the study provides physical insight that supports the development of more accurate and intelligent DED processes for high-precision manufacturing and aerospace component repair.

2 Research methods

This study adopts a numerical simulation approach to investigate powder flow characteristics and deposition profile evolution in DED process. The discrete coaxial nozzle configuration and varied injection angles are modeled to understand the influence of inclination on particle trajectories and substrate deposition behavior, particularly in remanufacturing contexts involving tilted surfaces. The simulation-based design is chosen due to its ability to isolate key process parameters and visualize complex flow behavior without the limitations and costs of physical experiments.

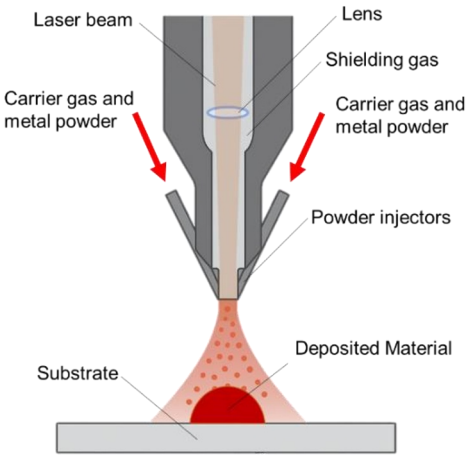

Fig. 1. The cross-section of discrete coaxial nozzle.

The simulation focuses on a powder stream projected through a discrete coaxial nozzle, where powder is injected via multiple off-axis ports surrounding a central beam path. This configuration reflects current trends in industry-driven DED systems used for component repair, especially in aerospace applications.

The substrate is modeled with an inclination to simulate common real-world re-manufacturing scenarios where damaged surfaces are not parallel to the nozzle axis. Numerical simulations were conducted using the Euler-Lagrange approach to capture the interaction between the carrier gas flow and the injected metal powder particles in a turbulent regime. The study investigates the influence of varying injection angles and surface inclinations on the deposition profile and particle behavior in DED process.

Table 1. Bulk aggregation properties of metal powders.

Properties	Setup
Granular Viscosity	gidaspow
Granular bulk viscosity	constant
The collision force between particles	Restitution coefficient 0.9
Packing limit	0.63
Radial distribution	Lun-et-al
Model	Multiphase Eulerian

2.1 Computational model

Computational modeling employed the Discrete Phase Model (DPM) to simulate powder trajectories, dispersion, and concentration. A three-dimensional domain of the nozzle–substrate system was developed based on geometrical parameters derived from previous experimental literature.

Table 2. Phase conditions.

Parameter	Phase 1	Phase 2
Type of material	Argon (gas)	Nickel powder
ρ (kg/m^3)	1.6228	8,902
Particle size (m)	-	6.5×10^{-5} – 8.5×10^{-5}
Inlet velocity (m/s)	4.4	3

2.1.1 Governing equations

The simulation employs a multiphase approach, solving the governing equations for the continuous gas phase and tracking discrete metal powder particles. The flow is modeled as incompressible and Newtonian with turbulence captured using the realizable k–ε turbulence model. The computational domain includes a nozzle, powder stream, and a tilted substrate.

a. Continuity Equation:

$$\frac{\partial \rho}{\partial t} + \nabla \cdot (\rho u) = 0 \tag{1}$$

b. Momentum Equation (Navier-Stokes):

$$\rho\left(\frac{\partial u}{\partial t} + u \cdot \nabla u\right) = -\nabla P + \nabla \cdot \tau + \rho g + F \tag{2}$$

c. Energy Equation:

$$\frac{\partial (\rho E)}{\partial t} + \nabla \cdot (\rho u E) = -\nabla \cdot q + \tau : \nabla u + Q \tag{3}$$

2.1.2 Turbulence Modeling

Turbulence was modeled using the realizable k–ε approach, which effectively represents recirculating and swirling flows in powder-laden jets. It provides accurate predictions of turbulent kinetic energy and dissipation rate, essential for analyzing powder dispersion and focal

convergence in the Directed Energy Deposition process through its two transport equations.

a. Turbulent Kinetic Energy (k):

$$\frac{\partial(\rho k)}{\partial t} + \nabla \cdot (\rho k u) = P_k - \rho\epsilon + \nabla \cdot (\sigma_k \mu_t \nabla k) \quad (4)$$

b. Turbulent Dissipation Rate (ε):

$$\frac{\partial(\rho\epsilon)}{\partial t} + \nabla \cdot (\rho\epsilon u) = C_1 \frac{\epsilon}{k} P_k - C_2 \rho \frac{\epsilon^2}{k} + \nabla \cdot (\sigma_\epsilon \mu_t \nabla \epsilon) \quad (5)$$

The model uses empirical constants $C_1 = 1.44$; $C_2 = 1.92$; $\sigma_k = 1.0$; $\sigma_\epsilon = 1.3$.

2.1.3 Discrete phase modeling

The simulation utilized Argon gas as the carrier gas, with boundary conditions set to mimic realistic industrial settings (i.e., velocity inlet for powder and gas, pressure outlet, and no-slip wall conditions). The powder material was modeled as Nickel particles with a diameter range of 65–85 μm and a density of 8,902 kg/m³.

Table 3. Powder flow simulation parameters.

Parameter	Setup
Model	Multiphase Eulerian
Viscosity	Realizable k-ε
Time step	$\alpha_{110°}$ = 0.000230 sec $\alpha_{120°,125°}$ = 0.000240 sec $\alpha_{130°,135°}$ = 0.000245 sec
Mesh quality	High-resolution mesh

Particle trajectories, stream convergence, and focal diameter were extracted for each injection angle scenario. Metal powder particles are modeled using a Lagrangian framework. The motion of each particle is calculated by Newton's second law:

$$\frac{du_p}{dt} = \frac{1}{m_p}(F_D + F_G + F_O) \quad (6)$$

Where F_D is the drag force; F_G is the gravitational force, and F_O represents other forces (e.g., lift).
Drag force:

$$F_D = \frac{1}{2} C_D \rho_g A_p (u_g - u_p)|u_g - u_p| \quad (7)$$

Drag coefficient (Schiller-Naumann):

$$C_D = \frac{24}{Re}(1 + 0.15 Re^{0.687}) \quad (8)$$

with:

$$Re = \frac{\rho_g d_p |u_g - u_p|}{\mu_g} \quad (9)$$

2.2 Simulation setup

To ensure reliability, mesh sensitivity analysis was performed, and simulation parameters were cross-referenced with validated data from previous DED modeling. The simulation workflow was repeated multiple times for consistency, and streamline visualizations were used to interpret the influence of each parameter on deposition behavior. Two independent variables are investigated:

- Injection Angles (α): 110˚, 120˚, 125˚, 130˚, 135˚
- Surface Inclinations (β): 0˚, 20˚, 40˚, and 60˚

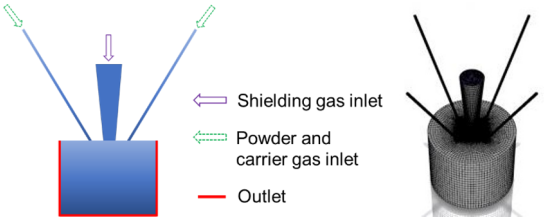

Fig. 2. Boundary condition and meshing.

Each combination of these parameters is simulated to analyze their influence on powder concentration, stream divergence, and focal point formation on the tilted substrate.

2.3 Deposition profile analysis

To study the deposition profile evolution, the particle concentration and trajectory data are projected onto the inclined surface. The substrate is discretized into grid cells where deposition flux is accumulated over time. The heat source and laser-material interaction are not explicitly modeled, focusing instead on powder trajectory and collision behavior.

Table 4. Deposition profile simulation parameters.

Property	Value	Unit
Liquidus temperature	1809	K
Solidus temperature	1776	K
Latent heat of fusion	271,960	J/kg
Standard state enthalpy	3.29e + 08	J/kg mol
Viscosity	0.0014	kg/m s
Thermal conductivity	43	W/m K
Specific heat	658	J/kg K
Surface tension coefficient	0.4	N/m

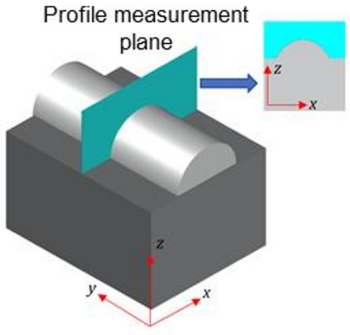

Fig. 3. 2D Profile measurement plane of DED deposition.

The resulting deposition profiles are analyzed to identify: peak deposition zone, effective deposition footprint, influence of gravity, surface normal misalignment, and flow deflection and divergence due to inclination.

2.4 Model validation

Model validation was performed by comparing the simulated deposition density and focal point diameter with experimental data from prior studies. Validation focused on powder flow convergence, focus width, and capture efficiency at varying injection angles. Simulations yielded turbulence intensity ranging from 0.42 to 1.05 at the nozzle exit and up to 1.26 at the aggregation zone (Fig. 7), matched with literature [15].

This methodology offers a detailed yet replicable approach to exploring the interplay between discrete coaxial injection angles and tilted substrates in powder-fed DED. By simulating key interactions, the study provides insights into optimizing nozzle configuration and positioning for enhanced material efficiency and geometric precision in aerospace remanufacturing tasks.

3 Results

The simulation results illustrate how different powder injection angles influence particle behavior within a discrete coaxial nozzle. The analysis covers deposition profile evolution, particle trajectories, and concentration distribution at various stand-off distances. Key parameters assessed include powder velocity, focal diameter, and stream convergence. Results from the Discrete Phase Model (DPM) simulation are compared across five distinct injection angles.

3.1 Focal point stand-off distance

Stand-off distance refers to the vertical distance from the nozzle outlet to the powder convergence zone. As illustrated in Fig. 4.

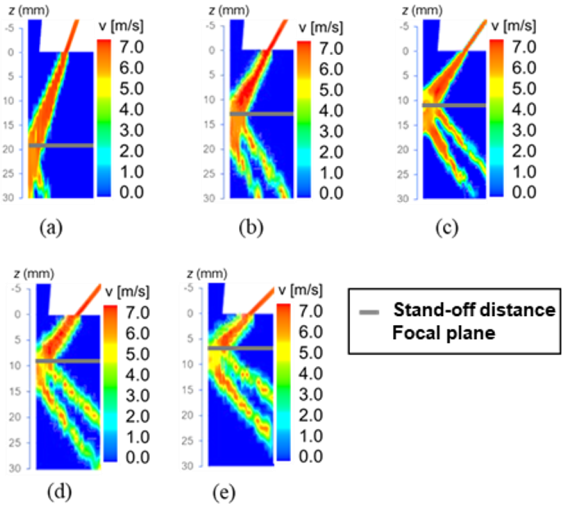

Fig. 4. Stand-off distance trajectory of the outlet nozzle in different injection angle: (a) α = 110°, (b) α = 120°, (c) α = 125°, (d) α = 130°, and (e) α = 135°.

Stand-off distances decrease with increasing injection angles: 19.36 mm (110°), 14.21 mm (120°), 10.14 mm (125°), 9.53 mm (130°), and 7.52 mm (135°). Wider injection angles yield more dispersed flows and less defined convergence zones. Discrete nozzles do not always form ideal convergence due to their stream geometry. At 130°, for instance, the flattening of the flow makes it difficult to form a precise focal point, as seen by elongated green contours. Optimizing stand-off distance is essential for achieving high deposition efficiency, which typically corresponds to the region of maximum powder mass concentration.

3.2 Powder velocity magnitude

Figure 5 qualitatively illustrates powder velocity magnitude across all nozzle variations. While the general flow remains consistent, particle velocity decreases with longer convergence paths. Higher injection angles result in lower central focal point velocities due to particle collisions and turbulence.

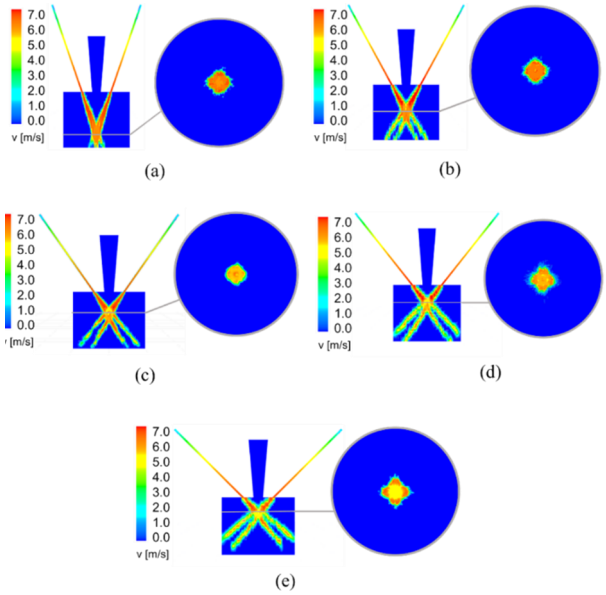

Fig. 5. Powder velocity magnitude in different injection angle: (a) α = 110°, (b) α = 120°, (c) α = 125°, (d) α = 130°, and (e) α = 135°.

From the top-view circular planes, it is evident that acute angles (e.g., 110°) produce higher velocities as particles travel more directly toward the substrate. Conversely, wider angles (130°, 135°) show greater dispersion and contour overlap due to increased collisions. Figure 19 confirms that powder velocity increases along the nozzle channel and peaks at the outlet. However, focal plane measurements reveal lower centerline velocities due to angled particle impacts and stand-off distance effects.

3.3 Powder mass concentration

Figure 6 shows powder concentration across different nozzle angles, with top-view contours highlighting horizontal distribution. The peak powder mass concentration is observed at higher injection angles due

to their shorter stand-off distances, leading to tighter focus zones.

Figure 8 reveals consistent concentration distributions, with core areas exhibiting high accumulation. The trend is more pronounced at acute angles where the vertical focal zone is more extended. This aligns with particle behavior seen in real conditions, where size variation and random flow patterns affect initial ejection.

Powder mass concentration trends are further detailed in Fig. 8, plotted against the Z-axis distance. Variations at 110° and 120° show broader concentration peaks, providing greater flexibility in vertical positioning. In contrast, angles like 130° and 135° yield higher peak values but less vertical tolerance. These differences are crucial in determining optimal working distances and avoiding overlap-induced dispersion.

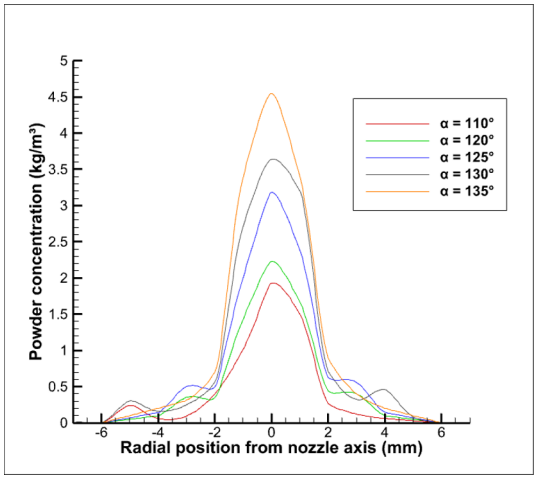

Fig. 6. Particle concentration on horizontal focal plane.

Powder flow behavior, including velocity, turbulence (Fig.7), focal distance, and mass concentration, is highly sensitive to injection angle. These findings provide essential insights for optimizing nozzle design in directed energy deposition systems and improving powder utilization and deposition quality.

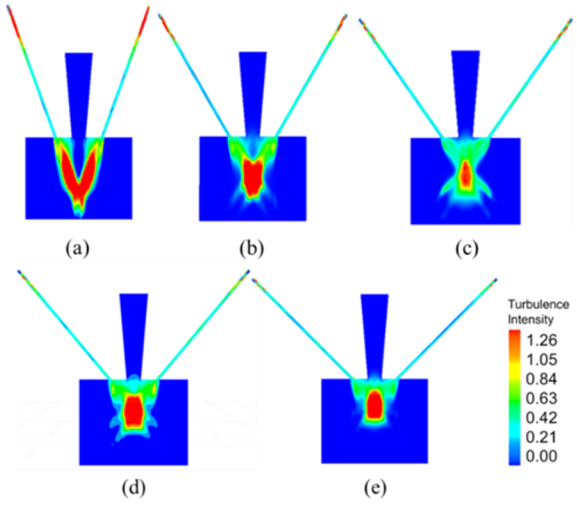

Fig. 7. Turbulence intensity in different injection angle: (a) α = 110°, (b) α = 120°, (c) α = 125°, (d) α = 130°, and (e) α = 135°.

The results indicate that powder flow behavior in discrete coaxial DED is intricately affected by the interaction between injection angle, particle size, and geometric stream convergence. Lower injection angles such as 110° facilitate a more direct path to the substrate, minimizing interparticle collisions and reducing turbulence intensity, which stabilizes the powder stream and sharpens the focal zone. This effect is particularly beneficial for deposition consistency and surface precision, especially in remanufacturing where dimensional fidelity is critical [16], [17], [18].

In contrast, higher angles (130° and 135°) exhibit reduced stand-off distances but suffer from dispersion and unstable convergence due to angular collision vectors and radial turbulence build-up. Despite their tighter focus zones, these configurations produce elevated peak concentrations with limited vertical tolerance, reducing the adaptability of the process across varying surface geometries.

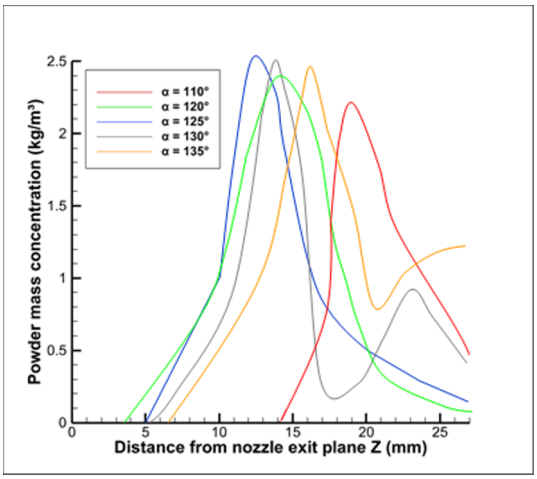

Fig. 8. Particle concentration as a function of the distance from nozzle exit plane Z.

The simulation confirms that turbulence intensity and powder mass concentration must be interpreted as nonlinearly related to angle, with convergence behavior being a function of both inertial trajectory and volumetric flow overlap. These findings reinforce the necessity of full-geometry modeling rather than sectional simplifications, emphasizing that accurate deposition behavior emerges from simulating the complete interaction of nozzle design, particle dynamics, and spatial constraints.

3.4 Deposition profile evolution

When depositing on an inclined substrate, gravity influences the melt pool with two components: a downward force ($g \cos \beta$) anchoring the pool to the surface, and a sideward force ($g \sin \beta$) causing lateral flow [19], [20]. This results in asymmetrical deposition shapes. As shown in Fig. 9, deposition profiles become increasingly distorted with greater inclination angles (0°, 20°, 40°, and 60°), confirming the direct effect of substrate tilt on geometry evolution.

Orthogonal simulation results (Fig. 9) reveal that increasing tilt angle leads to broader cladding width and

more significant peak shifting. Cladding width grows steadily with inclination, while peak shift initially increases before declining after 40°. For tilt angles under 20°, layer height remains stable, but beyond this point, height gradually decreases due to asymmetric melt flow and gravitational distortion. At 40°, side width reaches a maximum, reflecting a critical point where both melt pool dynamics and gravitational pull are strongly unbalanced.

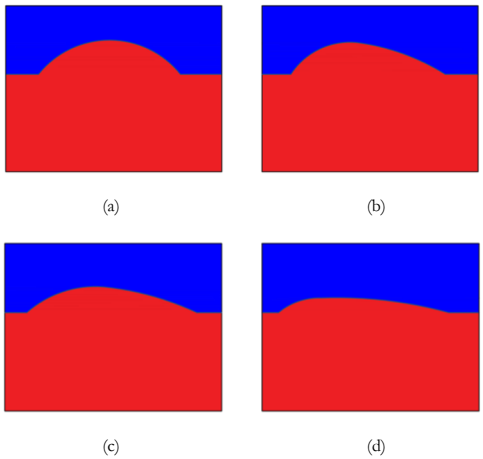

Fig. 9. Deposition profiles at different surface inclinations: (a) 0°, (b) 20°, (c) 40°, and (d) 60°.

Elevation side width increases beyond 40°, while reduced side depth and cladding height decline, indicating instability in deposition uniformity. Among all geometric aspects, cladding width and peak shift show the highest sensitivity to inclination, while depth and elevation evolve more moderately.

As demonstrated in Fig. 9, deposition begins deforming from the peak region when inclination surpasses 20°, with major width changes occurring at 40°. Below this threshold, the cladding maintains dimensional symmetry, and deviation in peak position remains below 15% of total width. This validates the reliability of the model for surface inclinations under 40°, where flow remains predictable. Predictive accuracy declines beyond 40° due to asymmetric powder accumulation and flow divergence. Fig. 30 further confirms that cladding width is most affected by tilt, compared to other parameters (Fig. 10).

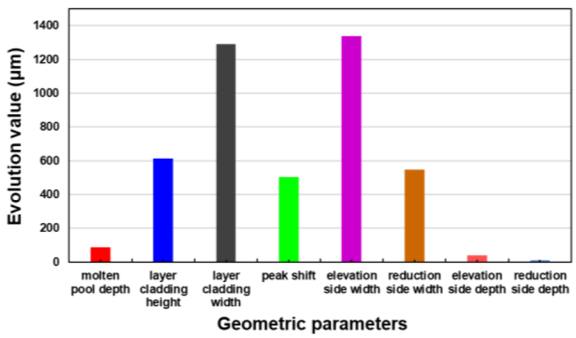

Fig. 10. The influence of tilt angle on geometric parameters.

These insights indicate that controlling inclination angle below 40° is key for maintaining deposition quality in multi-axis DED. Future studies should integrate multi-track simulations, dynamic melt pool behavior, and key forces such as Marangoni effect, Darcy flow, and capillarity [21], [22], [23]. Evaluating nozzle configurations and energy efficiency will also be essential to optimize powder delivery and improve predictive modeling in real applications.

4 Analysis and discussion

4.1 Main findings

Simulation results confirm that powder-injection angle is the dominant factor controlling flow stability and deposition focus. Narrower angles (110°–120°) generate a well-collimated stream with lower turbulence intensity, while wider angles (≥130°) increase particle collisions and radial dispersion. The observed relationship between stand-off distance and focal quality agrees with aerodynamic-focusing behavior in multiphase jets.

4.2 Comparison with previous studies

The obtained results are consistent with previous investigations [24], [25], which reported that increasing the outlet or injection angle in discrete-nozzle configurations leads to higher powder-stream divergence and a reduction in capture efficiency. This phenomenon is primarily attributed to intensified interparticle collisions and radial deflection of the carrier flow at larger ejection angles. Prior studies also confirmed that local turbulence intensity is a key factor influencing powder concentration and deposition uniformity in DED systems, indicating that minor geometric variations can significantly alter material delivery performance.

In contrast, the present study provides a coupled quantitative assessment of both injection-angle variation and substrate inclination. The combined effect of these parameters was found to control focal-zone convergence and layer geometry more strongly than either factor alone. This analysis extends the current understanding of discrete coaxial deposition by clarifying how angular misalignment modifies the particle momentum balance and shifts the effective deposition footprint, thereby advancing the physical interpretation of powder-flow dynamics in multi-axis DED applications.

4.3 Process implications and limitations

Practically, maintaining the injection angle below 120° enhances deposition efficiency and minimizes powder waste, providing guidance for adaptive nozzle-control strategies in industrial DED applications. Substrate inclinations exceeding 40° significantly distort layer geometry, indicating a geometric threshold for stable multilayer deposition.

The strength of this study lies in its comprehensive three-dimensional modeling of powder flow under realistic process parameters. Nevertheless, the current simulation does not include thermal interaction with the

laser or melt-pool dynamics; thus, future experimental validation is needed to verify the physical accuracy of the predicted flow patterns.

5 Conclusion

This study examined the influence of powder-injection angle and substrate inclination on powder-flow behavior and deposition morphology in Directed Energy Deposition using a discrete coaxial nozzle. Lower injection angles (≤120°) produced more stable and focused powder streams with improved deposition uniformity, while higher angles (≥130°) generated greater turbulence and dispersion. Substrate inclinations above 40° led to notable geometric distortion, confirming their critical effect on cladding precision.

The results establish a predictive understanding of powder-flow dynamics as a coupled function of injection geometry and surface orientation, providing theoretical and practical insight for the design of adaptive DED systems. The main limitation of this work lies in the absence of experimental validation. Future research will focus on laboratory-scale verification and the integration of AI-based monitoring for real-time process control. Overall, this study advances current knowledge of discrete coaxial deposition by clarifying how geometric parameters govern powder-stream stability and layer formation in multi-axis DED applications.

With sincere gratitude, the author acknowledges the funding support from IPPI Universitas Negeri Surabaya and simulation data guidance from National Central University. All data are available upon reasonable request. The author solely conducted the research, including concept development, simulation, analysis, and manuscript preparation.

References

1. L. DeWitte, C. Saldana, T. Kurfess, and K. Fu, Effect of coaxial nozzle wear on catchment efficiency in direct energy deposition built components. J. Manuf. Syst. **63**, 524–538 (2022). https://doi.org/10.1016/j.jmsy.2022.05.004
2. B. Han et al., Prediction of deposit characteristics based on the discrete coaxial nozzle during laser direct metal deposition. Opt. Laser Technol. **163**, 109385 (2023). https://doi.org/10.1016/j.optlastec.2023.109385
3. K. Wang et al., Powder stream performance of a novel annular laser direct metal deposition with inside-laser coaxial powder feeding nozzle: Simulation and experimental perspectives. Opt. Laser Technol. **175**, 110723 (2024). https://doi.org/10.1016/j.optlastec.2024.110723
4. F. Demir and O. Turgut, Study of heat transfer and flow field of coaxial round and swirl impinging jets on flat and finned plates via experimental and numerical approaches. Thermal Sci. Eng. Prog. **65**, 103867 (2025). https://doi.org/10.1016/j.tsep.2025.103867
5. A. Ramakrishnan, S. Kotha, A. Salem, and G. Dinda, Directed energy deposition of radially functionally graded nickel based superalloys IN625 and IN738: Microstructure and mechanical properties. J. Alloys Compd. **1016**, 178964 (2025). https://doi.org/10.1016/j.jallcom.2025.178964
6. J. Jang, Y. Shin, J. Lee, and S. H. Lee, Precipitation behavior and grain growth of Inconel 718 deposited by induction heating-assisted laser directed energy deposition. Addit. Manuf. **100**, 104678 (2025). https://doi.org/10.1016/j.addma.2025.104678
7. C. Guo, Y. Sun, Q. Li, H. Yue, and C. Wang, Analysis of the agglomeration of powder in a coaxial powder feeding nozzle used for laser energy deposition. Fluid Dyn. Mater. Process. **17**, 349–370 (2021). https://doi.org/10.32604/fdmp.2021.013535
8. X. Shi, D. Gu, G. Huang, and Y. Li, Laser directed energy deposition remanufacturing of LPBF-processed TA15 parts: Hybrid process interface induced microstructure inheritance and mechanical performance. J. Mater. Res. Technol. **33**, 3000–3011 (2024). https://doi.org/10.1016/j.jmrt.2024.10.018
9. S. A. Khairallah et al., High fidelity model of directed energy deposition: Laser-powder-melt pool interaction and effect of laser beam profile on solidification microstructure. Addit. Manuf. **73**, 103684 (2023). https://doi.org/10.1016/j.addma.2023.103684
10. A. López-Martínez et al., Modeling and comparison of the powder flow dynamics for tilted annular and discrete-outlet nozzles in laser directed energy deposition. J. Manuf. Process. **99**, 687–704 (2023). https://doi.org/10.1016/j.jmapro.2023.05.039
11. S. J. L. Bremer, M. Luckabauer, and G. R. B. E. Römer, Laser intensity profile as a means to steer microstructure of deposited tracks in directed energy deposition. Mater. Des. **227**, 111725 (2023). https://doi.org/10.1016/j.matdes.2023.111725
12. M. O. Gushchina et al., Features of the Ti-6Al-4V microstructure and phase composition formation by changing the thermal cycle during the process of direct energy deposition. Mater. Charact. **227**, 115330 (2025). https://doi.org/10.1016/j.matchar.2025.115330
13. H. Liu, H. Chen, and J. Xiong, Abnormal melt pool behavior in overhead wire arc-based directed energy deposition. J. Manuf. Process. **150**, 1164–1177 (2025). https://doi.org/10.1016/j.jmapro.2025.07.020
14. W. Zhang et al., Microstructural evolution and mechanical property enhancement: Thin-walled structures of an Inconel 718 superalloy fabricated via hybrid laser–arc directed energy deposition. Mater. Sci. Eng. A **940**, 148522 (2025). https://doi.org/10.1016/j.msea.2025.148522
15. Q. Liu, W. Li, K. Yang, Y. Gao, L. Wang, and X. Chu, Analytical investigation into the powder distribution and laser beam-powder flow interaction

in laser direct energy deposition with a continuous coaxial nozzle. Adv. Powder Technol. **34**, 104058 (2023). https://doi.org/10.1016/j.apt.2023.104058

16. H. S. Kim and S. H. Park, Influence of high powder flow dynamics on the efficiency of laser-directed energy deposition. Mater. Des. **255**, 114145 (2025). https://doi.org/10.1016/j.matdes.2025.114145.
17. S. B. Lawson, D. Yan, A. Tabei, B. K. Paul, and S. Pasebani, Numerical modeling of coaxial wire-powder laser directed energy deposition process in dissimilar metal additive manufacturing. Results Mater. **26**, 100701 (2025). https://doi.org/10.1016/j.rinma.2025.100701
18. M. Ostolaza, A. Urresti, J. I. Arrizubieta, A. Lamikiz, and M. Ortiz, CFD simulation for the modelling of the powder flow on continuous coaxial nozzles in the laser DED process. Procedia CIRP **111**, 282–286 (2022). https://doi.org/10.1016/j.procir.2022.08.022
19. E. Kim et al., Effects of growth rate and dynamic substrate tilt on properties of Au-Ta alloy films deposited by high-power impulse magnetron sputtering. Surf. Coat. Technol. **493**, 131231 (2024). https://doi.org/10.1016/j.surfcoat.2024.131231
20. P. Zhao, H. Wei, K. Zheng, Y. Lei, B. Li, and Y. Zhang, Modeling method for predicting part-scale geometric morphology considering manufacturing system states of laser-based directed energy deposition. Opt. Laser Technol. **192**, 113531 (2025). https://doi.org/10.1016/j.optlastec.2025.113531
21. J. Tu et al., Microstructure evolution and mechanical properties of Al0.5CoCrFeNi high-entropy alloy fabricated by direct energy deposition. J. Alloys Compd. **1036**, 181620 (2025). https://doi.org/10.1016/j.jallcom.2025.181620
22. Y. Wu, K. Liu, J. Li, J. Wang, and N. Soboleva, A review on formation and suppression mechanisms of porosity and cracks in wire arc-directed energy deposition Al-Zn-Mg-Cu alloys. J. Manuf. Process. **148**, 173–211 (2025). https://doi.org/10.1016/j.jmapro.2025.05.017
23. Y. Mao, H. Chen, and J. Xiong, A novel pre-melted liquid filler laser directed energy deposition for Al alloy: Process behaviors and filler transfer characteristics. Int. J. Heat Mass Transf. **252**, 127431 (2025). https://doi.org/10.1016/j.ijheatmasstransfer.2025.127431
24. M. Ostolaza, J. I. Arrizubieta, and A. Lamikiz, CFD modelling of the powder segregation in multi-material laser directed energy deposition. Int. J. Therm. Sci. **198**, 108885 (2024). https://doi.org/10.1016/j.ijthermalsci.2024.108885
25. T. Mede and M. Godec, Relevance of inter-particle interaction in directed energy deposition powder stream. Powder Technol. **435**, 119393 (2024). https://doi.org/10.1016/j.powtec.2024.119393